May 27, 2026

Intra- and Interannual Dynamics of Remotely Sensed Functional Diversity in Temperate Forests from Sentinel-2 Time Series

Isabelle S. Helfenstein[a*], Tiziana L. Koch[a,b], Meredith C. Schuman[a,c], Felix Morsdorf[a]

[a]Remote Sensing Laboratories, Department of Geography, University of Zurich, CH-8057 Zurich, Switzerland

[b]Swiss Federal Institute for Forest, Snow and Landscape Research WSL, CH-8903 Birmensdorf, Switzerland

[c]Department of Chemistry, University of Zurich, CH-8057 Zurich, Switzerland

[*]Corresponding author. Email address: isabelle.helfenstein@geo.uzh.ch

Abstract

Monitoring biodiversity change requires approaches that capture ecological dynamics across space and time. Satellite remote sensing provides unique opportunities for such monitoring, but most studies of functional diversity rely on single-date imagery, typically at peak greenness, neglecting seasonal variability. Here, we used multi-year, dense Sentinel-2 time series (2017–2021) to assess seasonal and interannual dynamics of trait-related spectral indices (CIre, CCI, and NDMI) and associated functional diversity metrics (richness and divergence) of temperate mixed forests in northeastern Switzerland as a case study. Seven-day composites were analyzed to characterize intra- and interannual trajectories and to compare patterns across different forest communities. We show that all indices and metrics exhibit substantial seasonal and interannual variation, with important deviations from peak greenness values. Needle-dominated stands displayed higher functional diversity metrics than broadleaf stands, likely partly reflecting canopy structural effects, while functional divergence remained comparatively consistent over the years and communities. These results demonstrate that accounting for temporal dynamics is essential to accurately characterize forest functional diversity from space. Sentinel-2 time series offer a promising basis for biodiversity assessments and can complement field and airborne approaches in assessing forest dynamics.

KEYWORDS functional diversity, temperate forests, phenology, spectral indices, biodiversity monitoring, Sentinel-2

1 Introduction

Quantifying biodiversity change is essential to assess ecosystem state and trends, understand the impacts of climate change and human activities, and inform policy decisions for biodiversity conservation (Schmeller, 2008; Rodríguez-Ezpeleta *et al.*, 2021). However, ground-based biodiversity data are often limited to small regions of interest or single temporal snapshots and may be biased by experimental designs (Laureto *et al.*, 2015). Standardized, scalable approaches and improved data integration are needed to ensure high data quality with sufficient spatial and temporal coverage (Schmeller, 2008; Gonzalez *et al.*, 2023).

The Sentinel-2 satellite constellation provides capabilities for large-scale vegetation monitoring through repeated standardized data acquisition. With a spatial resolution of 10–20 m, a revisit frequency of five days at the equator, and dedicated red-edge and short-wave infrared bands, it enables the assessment of key physiological properties such as leaf area index and chlorophyll content (Immitzer *et al.*, 2016; Phiri *et al.*, 2020; Delegido *et al.*, 2011). Sentinel-2 has been widely applied in agriculture and forestry, supporting applications ranging from crop monitoring to forest classification, biomass estimation, and disturbance assessment (Segarra *et al.*, 2020; Rüetschi *et al.*, 2021; Lang *et al.*, 2019; Sturm *et al.*, 2022; Blickensdörfer *et al.*, 2024).

Beyond structural and productivity measures, Sentinel-2 also enables the study of vegetation dynamics through phenology and spectral index-based approaches. Phenology, the study of the timing of reoccurring biological events (Rosenzweig *et al.*, 2008) is a key component and indicator of biodiversity (Morellato *et al.*, 2016; Viña *et al.*, 2016; O'Connor *et al.*, 2020). Land surface phenology (LSP), the phenology of vegetated surfaces observed from satellites, has been recognized as a priority biodiversity variable for space-based monitoring (Skidmore *et al.*, 2021). LSP both responds to, and influences weather and climate (Garonna *et al.*, 2018), and is commonly derived from satellite time series of vegetation indices such as normalized difference vegetation index (NDVI) (Forkel *et al.*, 2013). These time series allow the detection of phenological stages (e.g., onset of the growing season, senescence) and the evaluation of trends across multiple years (Zhou *et al.*, 2020; Garonna *et al.*, 2016; Vitkovskaya *et al.*, 2016).

While phenology captures the timing of vegetation activity, functional diversity provides complementary information on the range of plant strategies within communities. Using functional diversity approaches, the diversity of traits (observable characteristics of organisms (Violle *et al.*, 2007)) can be quantified within a plant community or ecosystem. Although a positive linear relationship often exists between plant functional and taxonomic diversity, functional diversity quantifies the number of plant strategies rather than the number of coexisting species (Gazol & Camarero, 2016).

Trait-based diversity, often referred to as functional diversity, has recently been assessed from satellite remote sensing using plant trait maps or vegetation indices related to pigmentation, water content, and productivity as a basis

(Hauser *et al.*, 2021; Rossi *et al.*, 2020; Helfenstein *et al.*, 2022). Previous studies showed that remote sensing can effectively link plant functional diversity patterns to ecosystem functions such as ecosystem productivity (Zheng *et al.*, 2023), ecosystem resilience (Helfenstein *et al.*, 2025), or land use, with undisturbed forests and logged forests showing higher diversity than oil palm plantations (Hauser *et al.*, 2022).

Remotely sensed functional diversity is derived in a multidimensional feature space using canopy traits derived from spectroscopy data by machine learning approaches such as partial least squares regression (PLSR) (Chlus & Townsend, 2022; Zheng *et al.*, 2023), model inversion (Hauser *et al.*, 2022), or spectral indices (Helfenstein *et al.*, 2025). These diversity metrics describe, for example, the community niche in terms of richness, linked to the spread of the derived values in the community space, and divergence, describing the distribution of the derived values in the community space.

The importance of temporal information for remote sensing of plant biodiversity has been highlighted in recent reviews (Wang & Gamon, 2019; Torresani *et al.*, 2024), which identify the season-dependence of spectral diversity metrics as a major unresolved knowledge gap. Several studies have shown that the relationship between spectral diversity and species richness varies across seasons, underlining the need to better understand the variation in timing and magnitude of spectral diversity metrics (Torresani *et al.*, 2019; Wang *et al.*, 2022; Fassnacht *et al.*, 2022). Recently, Chlus et al. 2022 (Chlus & Townsend, 2022) assessed seasonal variations of repeated remotely sensed trait estimations obtained from PLSR on high-resolution spectroscopy data. These variations potentially affect the resulting functional diversity maps. On one hand, the functional diversity of a forest canopy reflects its composition in terms of the number, density, and type of trees, which are not expected to change dynamically in short periods, such as within a single year, except in cases of severe disturbance (Lindenmayer *et al.*, 2019; Viljur *et al.*, 2022). On the other hand, traits are known to vary over the season, for example through temporal niche differentiation or through asynchrony (Huang *et al.*, 2019; Yuan *et al.*, 2019), but also due to phenology. However, existing knowledge of temporal variation in foliar traits is limited to a few species or small areas, largely due to the challenges of repeated *in situ* measurements (Chlus & Townsend, 2022).

Remote sensing of functional diversity has advanced in large part due to the availability of relevant measurements from the Sentinel-2 mission. These studies generally use Sentinel-2 measurements from a single mid-season time point to compare across regions and years, even though Sentinel-2 provides multi-year, dense time series data. It remains unclear how trait-related vegetation indices and associated diversity metrics assessed using Sentinel-2 vary seasonally and interannually. This limits our ability to evaluate their representativeness for biodiversity assessment and ecological interpretation.

Remotely sensed biodiversity maps in a community are typically determined during the time of peak standing biomass (Cornelissen *et al.*, 2003). Recent studies of functional diversity in temperate ecosystems have used remote

sensing data from June and/or July to represent peak greenness (PG) for a specific region (Schneider *et al.*, 2017; Helfenstein *et al.*, 2022), while times of very low cloud cover have been the focus in less seasonal regions (Hauser *et al.*, 2022). However, to our knowledge, there is a lack of studies evaluating the representativeness of PG for diversity measures. Recent studies have begun to explore the temporal dynamics of spectral and trait information using e.g. model-based trait trajectories from hyperspectral data (Mederer *et al.*, 2025) or multitemporal spectral diversity (Liu *et al.*, 2025). Nevertheless, it remains unclear how spectral indices and the corresponding commonly used diversity metrics derived from satellites are affected by the timing of the satellite acquisition and change during the growing season, and how suitable PG is as a reference time for long-term monitoring.

The dense revisit frequency of Sentinel-2 provides an opportunity to test the effect of seasonality or acquisition time point on functional diversity assessments. Here, we use Sentinel-2 time series to evaluate how the timing of satellite observations influences the representation of functional diversity in forest ecosystems, by focusing on the temporal behavior of trait-related spectral indices and derived diversity metrics to build the basis for their use as biodiversity indicators in monitoring approaches.

The aim of this study was to assess how seasonal and interannual dynamics of canopy trait-related spectral indices from multi-year, dense time series of Sentinel-2 influence apparent functional diversity patterns in temperate forests. Specifically, we quantified intra- and interannual variations in trait-related indices and corresponding index-based diversity metrics. We derived the red-edge chlorophyll index CIre, the chlorophyll carotenoid index CCI, and the normalized difference moisture index NDMI as the basis for the index-based functional diversity metrics richness and divergence every seven days over five consecutive years and evaluated their utility for biodiversity assessment across different forest communities. Trait-related spectral indices and derived diversity metrics may exhibit substantial seasonal and interannual variability, rather than remaining stable around peak greenness. Furthermore, seasonal dynamics and their interannual variability likely differ among forest communities due to differences in canopy composition and phenology. Understanding this variability is essential for multi-year functional diversity assessments, as peak greenness may not be a consistently representative time point, i.e. a seasonally stable and interannually consistent stage of the diversity metrics, reflecting a characteristic state rather than a transitional or extreme phase.

We address the following research questions: (i) What are intra- and interannual patterns of trait-related indices (red-edge chlorophyll index CIre, chlorophyll/carotenoid index CCI, and normalized difference moisture index NDMI) and corresponding index-based diversity metrics (richness and divergence) over a five-year period (2017–2021)? (ii) How representative is PG when assessing trait-related vegetation indices and index-based diversity metrics? (iii) How do intra- and interannual variations of index-based diversity metrics differ among forest communities?

2 Material and Methods

2.1 Study area

The study area encompasses a 900 km^2 tile (Figure 1) in northeastern Switzerland, mainly in the Canton of Zurich. According to the cantonal forest mask, the official forest mask polygons provided by the canton of Zurich (GIS-ZH, 2019), 27.42% (246.8 km^2) of the area is covered by temperate mixed forests. Elevation ranges from 374 to 895 m above sea level. The forests are potentially composed of European beech (*Fagus sylvatica*) and other broadleaf species (Bürgi & Schuler, 2003; Scherrer *et al.*, 2023). However, past management has introduced a high proportion of fast-growing conifers (*Picea abies, Abies alba*) outside of their natural range, increasing susceptibility to disturbances (Bürgi & Schuler, 2003; Schuldt *et al.*, 2020; Scherrer *et al.*, 2023). The main tree species in the Canton of Zurich are *P. abies*, *Fagus sylvatica*, *A. alba*, and *Fraxinus excelsior* (Baudirektion Kanton Zürich, 2020). Because this study focuses on the influence of maximum standardized temporal density of Sentinel-2 acquisitions, we selected a single focal 30 km x 30 km tile with a forest composition that is well characterized from inventory data. The results can be used as a basis to select temporal resolution and focal time periods across larger or less well characterized regions.

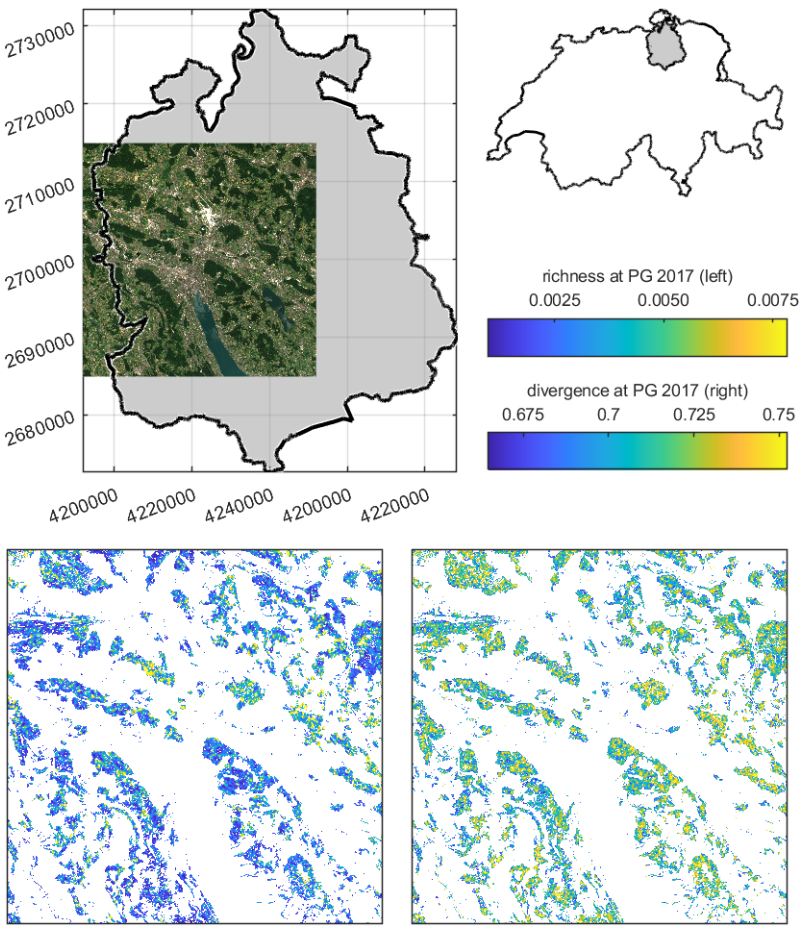

Figure 1: Study area. Top left: RGB Sentinel-2 image of the study area from June 19th, 2017. The black line indicates the cantonal border of Zurich using swissBOUNDARIES (swisstopo, 2021). Top right: Overview of location within Switzerland. Bottom left: Index-based functional richness map of the forested pixels in the study area calculated based on data from peak greenness (PG) in 2017 (July 2nd, 2017). Bottom right: Index-based functional divergence map of the forested pixels in the study area calculated based on data from PG in 2017 (July 2nd, 2017).

Canopy traits and spectral indices are affected by changes in weather conditions, such as temperature and precipitation (Maynard *et al.*, 2022; Hordijk *et al.*, 2025), especially at large spatial scales (Da *et al.*, 2022). Seasonal and interannual differences provide an important context for interpreting temporal variations in spectral indices related to canopy traits and functional diversity. The five years from 2017 to 2021 showed considerable variation in temperature and precipitation in the study area (Table 1). Specifically, 2017 was warmer than average in spring and summer, followed by a cooler and sunnier fall (MeteoSchweiz, 2018). In 2018, a record-breaking warm period and prolonged drought occurred, representing the most severe precipitation deficit in more than a century (MeteoSchweiz, 2019). Then, 2019 remained warm but with increased spring precipitation, supporting recovery from the previous year's drought (MeteoSchweiz, 2020a). Finally, 2020 included moderate summer heatwaves with heavy precipitation in August and October (MeteoSchweiz, 2021), while 2021 was characterized by cooler, wetter conditions in spring and summer and a drier, sunnier fall (MeteoSchweiz, 2022).

2.2 Sentinel-2 data and processing

We processed all available Sentinel-2 images from Level-1C onward in the FORCE software (v. 3.7.8-12; Frantz (2019)). We applied radiometric correction, including atmospheric and topographic correction, bidirectional reflectance distribution function (BRDF) correction, and adjacency effect correction, individually per image. We also removed areas covered by clouds with the improved version of Fmask (Frantz *et al.*, 2018; Zhu *et al.*, 2015) and buffered around clouds, shadows, and snow. Finally, the 10 m spatial resolution resampled images (3000x3000 pixels) were co-registered with Landsat Collection 2 near-infrared images from 2014–2021 to ensure spatial consistency (Rengarajan *et al.*, 2020; Rufin *et al.*, 2021). Sentinel-2 images covering Switzerland processed with FORCE can be accessed via Koch *et al.* (2024) and recently supported a wide range of applications and studies, such as grassland-use intensity estimation (Weber *et al.*, 2023), tree intraspecific variation (Koch *et al.*, 2025a) and phenology (Koch *et al.*, 2025b), and the relationship of stem-derived tree water deficit with vegetation indices (Bloom *et al.*, 2025).

Table 1: Weather summary focusing on temperature (T) and precipitation (P) for North/Mid-East Switzerland compared to average values from 1981–2010. Information collected from climate records (MeteoSchweiz, 2018, 2019, 2020a, 2021, 2022).

Season	2017	2018
Spring	+1.7°C	Mar -1°C, Apr +3.9°C, May +1.9°C
Summer	+1.9°C	+2°C
Fall	-0.3°C (cool start, warm Oct)	+1.8°C
Precipitation	-10% of average	-40% of average (dry Apr–Nov)

2019	2020	2021
average T	+1.8°C	-1.1°C
+2.3°C	+1°C, mild heatwaves	+0.5°C, very wet
+1.1°C, mixed P	+1°C	+0.5°C
average P	average P	+60% P

We generated multi-year, dense time series covering the study area with radial basis function (RBF) convolutional filtering (Schwieder *et al.*, 2016). Satellite time series contain noise introduced by, e.g., undetected clouds and varying atmospheric conditions, which can be reduced using smoothing functions (Lara & Gandini, 2016). The RBF is based on the original images and includes interpolation and smoothing using three differently weighted temporal moving windows with kernel widths of 7, 14, and 21 days. Within this step, we applied further quality checks and removed outliers from the time series due to clouds and cloud shadows, snow, saturation, or limited illumination. The generated time series of spectral indices, namely the NDVI, CIre, CCI, and NDMI (see below), consists of composites calculated in steps of 7 days. The processing thus produces weekly composites from an interpolated and smoothed time series. We thus derived 51 composites per year, resulting in a total of 255 composites during the observation period from 2017 to 2021.

We built our forest mask based on the forest area dataset provided by the canton of Zurich in the LV95 reference system (GIS-ZH, 2019). We first warped the data using gdal to match the projection of the Sentinel-2 data in WGS 84/UTM 32N (GIS-ZH, 2019). To ensure examination of intact green forest canopy (neither harvested nor disturbed), we adjusted the cantonal forest mask by using annual thresholds of the normalized difference vegetation index (NDVI, Eq. 1, bands 4 and 8) based on a median outlier function from composites of June/July. The NDVI thresholding reduced the cantonal forest mask by 12.2% to 216.8 km^2.

NDVI was calculated as

$$\frac{\rho_{842} - \rho_{664}}{\rho_{842} + \rho_{664}} \tag{1}$$

In addition to NDVI, we focused on time series of three spectral indices representing canopy traits: CIre, CCI, and NDMI, linked to chlorophyll content, carotenoid/chlorophyll ratio, and canopy water content. We selected these three trait-related indices because they are well suited to the spectral configuration of Sentinel-2, rely on distinct spectral bands, and have been previously tested and validated in temperate forest ecosystems. This combination is also supported by recent literature on Sentinel-2–based vegetation monitoring using dense time series (e.g., Guzmán Q. *et al.*, 2023; Bloom *et al.*, 2025) and functional diversity assessments (Helfenstein *et al.*, 2025).

We used the red-edge chlorophyll index (CIre, Eq. 2, bands 7 and 5) to estimate chlorophyll content (Gitelson *et al.*, 2003). CIre from Sentinel-2 showed a strong correlation with in-situ chlorophyll content in mixed mountain forests in southern Germany (Ali *et al.*, 2020).

CIre was calculated as

$$\frac{\rho_{783}}{\rho_{704}} - 1 \tag{2}$$

The Chlorophyll Carotenoid Index (CCI, Eq. 3, bands 3 and 4) is sensitive to carotenoid content relative to chlorophyll content (Springer *et al.*, 2017). CCI has been validated for pigment ratios (Gamon *et al.*, 2016; Wong *et al.*, 2020),

and time series of CCI have been successfully applied in real forest ecosystems to capture physiological changes in canopy pigment composition in North America (Guzmán Q. *et al.*, 2023).

CCI was calculated as

$$\frac{\rho_{560} - \rho_{664}}{\rho_{560} + \rho_{664}} \tag{3}$$

The Normalized Difference Moisture Index (NDMI, Eq. 4, bands 8A and 11), also called NDWI or NDII (Gao, 1996; Pan *et al.*, 2018), utilizes wavelengths in the NIR and SWIR bands to detect water content, the total amount of water in a leaf or canopy relative to its dry mass (Jetz *et al.*, 2016; Wang & Qu, 2007). Recent work in Swiss temperate forests further linked the NDMI band combination with drought response in Swiss forests (Sturm *et al.*, 2022) and with in-situ measurements of canopy water status (Bloom *et al.*, 2025). These studies showed that NDMI can capture multitemporal and seasonal dynamics in canopy water, supporting its suitability for time-series analyses in Central European forests.

NDMI was calculated as

$$\frac{\rho_{865} - \rho_{1614}}{\rho_{865} + \rho_{1614}} \tag{4}$$

2.3 Trait-related index-based diversity metrics

Two functional diversity metrics, functional richness and divergence, were calculated using MATLAB 2024b according to Schneider et al. Schneider *et al.* (2017) using the spectral indices as a basis. Both metrics are orthogonal, meaning they vary independently from each other and are not correlated (Mason *et al.*, 2005).

Richness is a measure of the community extent, describing the size of the feature space (see Figure 2), whose axes are defined by the three normalized traits (Villéger *et al.*, 2008; Schneider *et al.*, 2017). Richness is the volume of the mapped pixels' concave hull in multi-dimensional feature space using α-shapes (Gruson, 2020). Divergence measures the distribution of data points within the community niche and is sensitive to clumping. The divergence calculation results in one if all points are scattered equally far away from the common center in all trait axis directions (Villéger *et al.*, 2008; Schneider *et al.*, 2017). Divergence was calculated using the number of pixels mapped in the functional space (S), the Euclidean distance between every pixel i and the center of gravity (dGi), and the mean distance of all pixels to the center of gravity (dG) (Schneider *et al.*, 2017).

2.4 Characterization of the growing season

To enable better comparisons across years, we defined the growing season and derived phenological metrics for every year based on the NDVI (see Figures 2 and 3) using MATLAB 2024b. To ensure that all comparisons are made under leaf-on conditions, we only examined vegetation indices and diversity metrics from within the growing season.

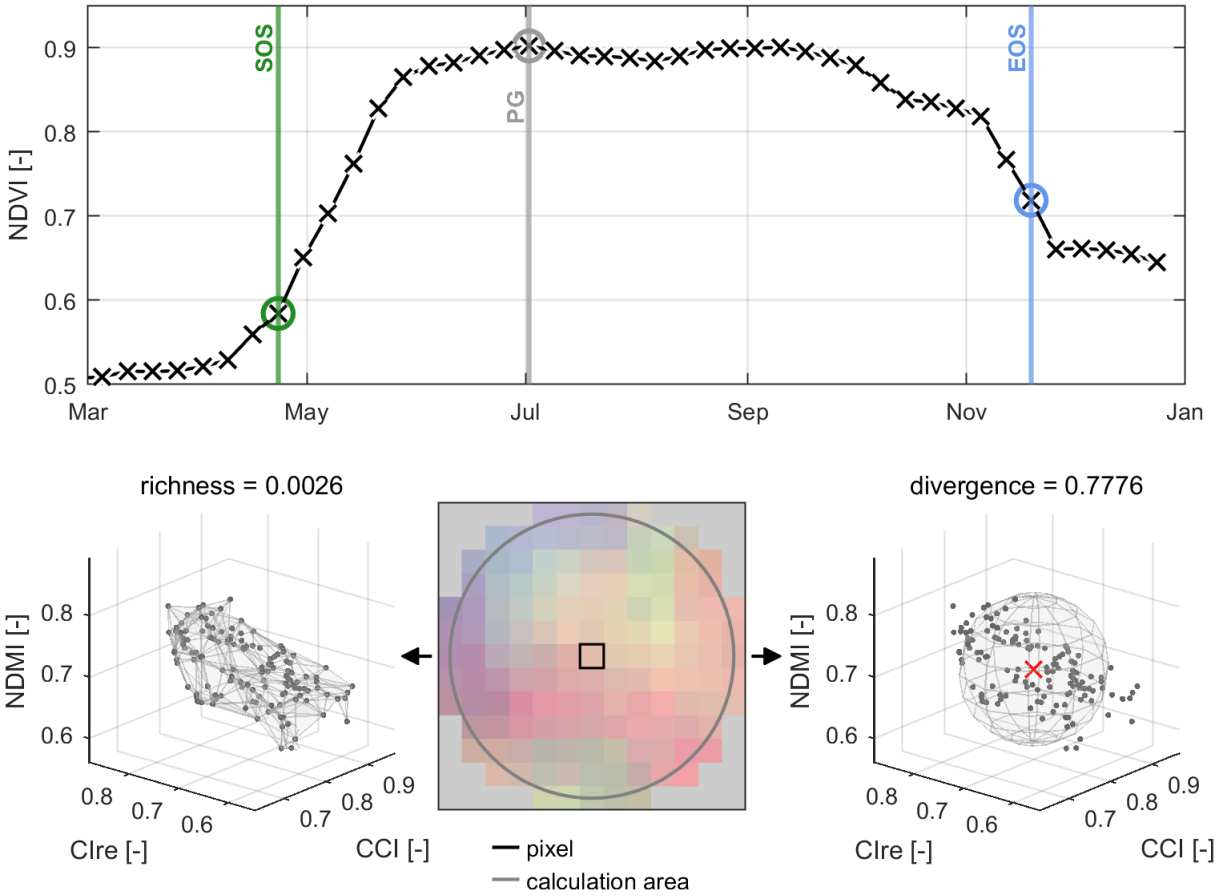

Figure 2: Methodological concepts. Top: Example of how to characterize the growing season with phenological metrics (start of season (SOS) and end of season (EOS)) using the derivative method on the NDVI time series. Additionally, peak greenness (PG), as the annual maximum, is derived. Bottom: Concept of functional diversity metrics calculation for every image and pixel based on a 60 m radius (middle). Functional richness (left) measures the niche extent based on the three vegetation indices, and functional divergence (right) measures the distribution within the occupied niche based on the three vegetation indices.

NDVI is commonly used as a proxy for the fraction of photosynthetically active radiation intercepted by vegetation (Wang *et al.*, 2004), which makes it an established index in land surface phenology studies and a valuable tool for determining the growing season and the green active forest canopy (Huemmrich *et al.*, 1999; Soudani *et al.*, 2012; Hmimina *et al.*, 2013).

We used the derivative or maximum increase/decrease method on the NDVI time series to derive the start of season (SOS) and the end of season (EOS), and the annual maximum NDVI value to derive peak greenness (PG) (White *et al.*, 2009; Garonna *et al.*, 2014). The derivative-based method provides a quantitative way to delineate the active phases of plant development within a pixel for a year. We applied the derivative method relative to the annual global maximum NDVI, identifying SOS and EOS as the dates of maximum rate of increase and decrease respectively, which avoids misidentification from local extrema in the smoothed time series and removes the need for a fixed threshold that would not be appropriate across pixels with varying NDVI ranges. We calculated the phenological metrics for each forested pixel (Broich *et al.*, 2014; Revermann *et al.*, 2016; Garonna *et al.*, 2016) and derived their respective day of year (DOY) (Forkel *et al.*, 2013; Buermann *et al.*, 2018; White *et al.*, 2009; Wu & Xin, 2022). The growing season length (GSL) was calculated as $GSL = EOS - SOS$. The timing of the phenological metrics varied across sites, and hence, we used the median phenological metrics per year. To enable better comparability, we finally used these phenological metrics to align the time series starting from the annual SOS.

2.5 Forest community analyses

To gain insight into differences in diversity metrics among forest communities, we analyzed the time series of five different forest communities based on aerial forest stand information provided by the canton of Zurich (GIS-ZH, 2023). For each community, we evaluated intra-seasonal dynamics of diversity metrics derived from the Sentinel-2 time series. We then decomposed the variance of these metrics into spatial, temporal, and interaction components, enabling us to disentangle intra-annual and interannual variability as well as differences among communities.

We gathered forest community information from the aerial forest stand dataset of the canton of Zurich (GIS-ZH, 2023), which contains forest stand attributes, including composition of tree species in increments of 10% (2000–2013). We classified each polygon based on the dominant tree species or species groups, using a threshold of 60% cover within polygons with at least 80% canopy cover. Specifically, polygons with at least 60% *F. sylvatica* were classified as *F. sylvatica*-dominated, those with at least 60% *P. abies* as *P. abies*-dominated, those with combined coniferous species (*P. abies, A. alba, Pinus sylvestris, Larix* spp., and other unspecified needle trees) as needle-dominated and those with combined broadleaf species as broadleaf-dominated. For analyzing forest communities per pixel, we considered the surroundings of at least 60 m to guarantee reliable diversity metrics. If an area fell into 40% evergreen and deciduous species, the pixel was classified as mixed.

We quantified the total variance and its spatial, temporal and interaction components for each forest community introduced by Rossi et al. Rossi *et al.* (2021) using the R package *stdiversity* (https://github.com/RossiBz/stdiversity, accessed on August 15, 2025). To minimize spatial autocorrelation, we selected pixels that were evenly distributed throughout the study area and not adjacent. Based on the minimum number of available pixels per community, we derived 133 pixels of the functional diversity metrics for each community, excluded the EOS image for the annual time series to avoid extrapolation of variance, and finally used them for the analysis.

3 Results

3.1 Characterization of the growing season

The annual median phenological metrics of the study area varied across years (Figure 3). The median dates of SOS shifted up to three weeks, with the earliest DOY in 2020 and the latest in 2019. PG remained the most stable with variations up to 16 days across years. EOS was detected with the greatest variation, ranging from DOY 281 to DOY 314. The longest growing season was observed in the years 2018 and 2020. Delays in all metrics by about 2–3 weeks were observed in 2019 and, apart from the PG, also in 2021.

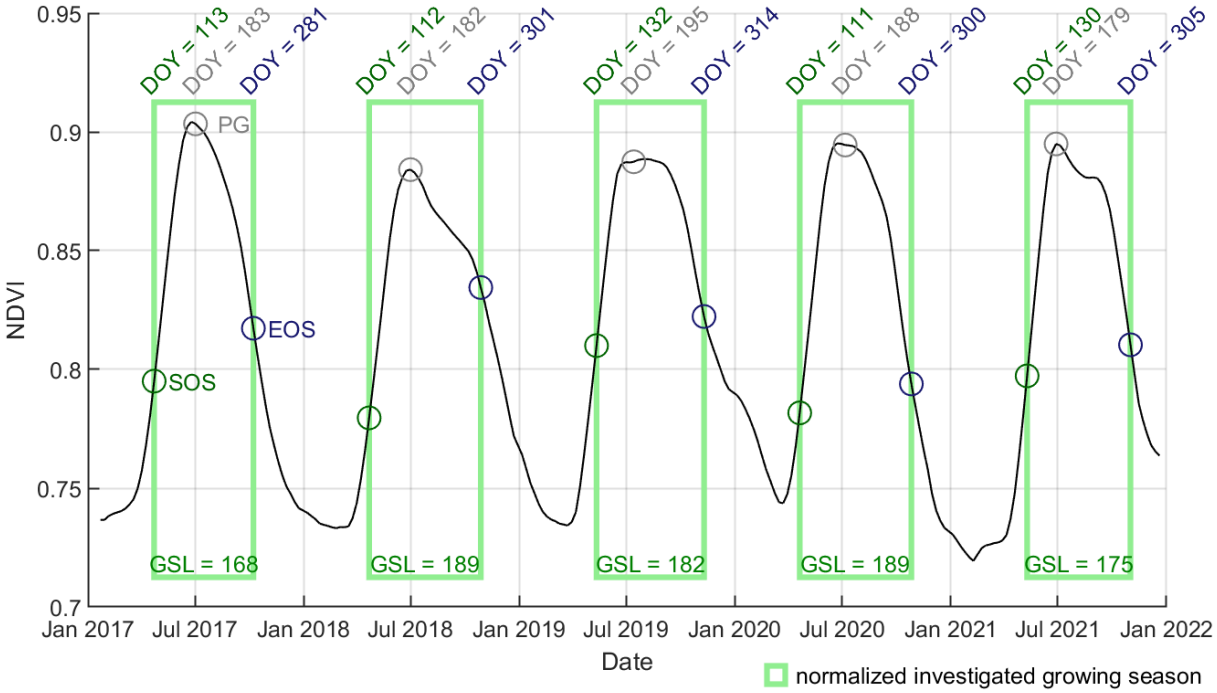

Figure 3: Derivation of phenological metrics from the mean 7-day NDVI time series for the whole study area. The derived phenological metrics are the start of season (SOS), the end of season (EOS), peak greenness (PG) and the growing season length (GSL). The GSL was used to normalize the investigated time series of the indices and diversity metrics.

3.2 Temporal variation of trait-related indices

To analyze the intra-annual and interannual patterns of trait-related indices that were used to derive functional diversity metrics, we used the yearly time series that were aligned with the yearly SOS. Figure 4 shows the mean time series of all years and their respective standard deviations, the yearly value distributions, and the evolution of the indices for all years separately.

All three indices typically increased in spring and decreased in fall (Figure 4). All curves exhibited an initial rapid rise shortly after SOS, followed by a peak around 4 weeks (CCI) or 8 weeks (CIre) after SOS and gradual decrease until about 20 weeks after SOS, or else a plateau (NDMI) from around 5 weeks until 22 weeks after SOS. The peak of CIre corresponded to PG, whereas both CCI and NDMI peaked before PG with NDMI remaining close to its maximum value at PG. Higher standard deviation among years compared to mid-season was observed for all three indices in the first weeks of the growing season (1–5 weeks after SOS) and towards the end of the season (20–25 weeks after SOS), with CCI showing the greatest standard deviation, particularly before week 13 after SOS and between 15–20 weeks after SOS (Figure 4).

We observed more specific differences in the distribution of index values across years (Figure 4). CIre displayed higher spring peaks in 2017 and 2021, causing a change in the shape of the intra-annual distribution of values towards a bimodal distribution. The lowest NDMI was recorded in July/August 2018 and 2020, resulting in a distinct peak

prior to the plateau in these years. Each year exhibited a peak in CCI within the first 5 weeks of the growing season and a second but lower peak in late summer around 16–21 weeks after SOS, latest in 2018. As 2017 had the shortest growing season, in this year the indices declined earliest in the fall, followed by 2020. Overall, the most variability across years was found for CCI (Figure 4).

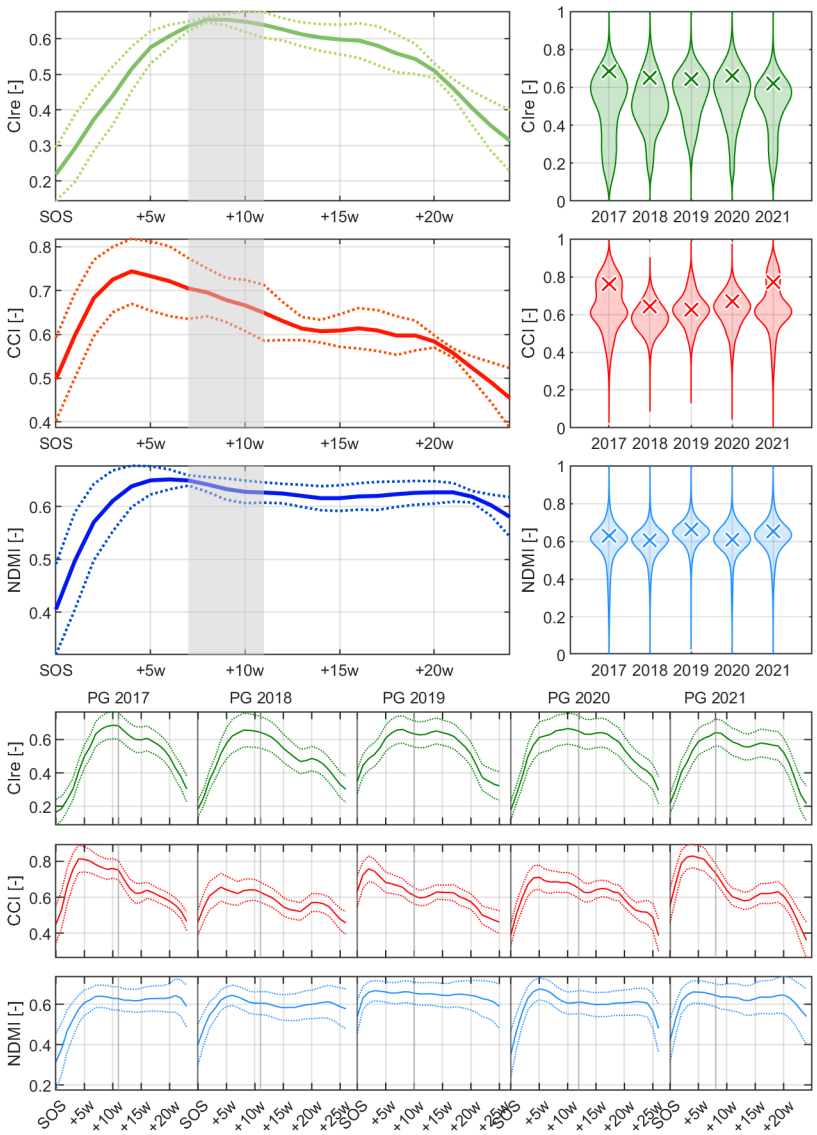

Figure 4: Temporal development of the three trait-related indices CIre (chlorophyll, green), CCI (carotenoid/chlorophyll, red), and NDMI (water content, blue) throughout the growing season. Top left: Mean index time series of all years (solid lines) and their respective standard deviations across years (dashed lines), each normalized to SOS. The gray area marks the range of the PG from all years (7–11 weeks after SOS). Top right: Distribution of index values during the entire growing season of each year for the whole study area as violin plots. Bottom: Temporal development of mean index time series (solid lines), separate for each year and the respective standard deviations (dashed lines).

3.3 Temporal variation of diversity metrics

Functional richness and divergence showed distinct intra-annual and interannual patterns when aligned with the yearly SOS (Figure 5). Richness increased for the first 5 weeks from SOS, although not as steeply as the trait-related indices (Figure 4), then remained roughly constant (albeit with some fluctuations) until about 21 weeks following SOS, after which it increased again, more steeply (Figure 5). An increase in interannual standard deviation around 15–18 weeks after SOS preceded the increase in mean richness. In contrast, divergence initially increased about as steeply as the individual index values but became roughly constant at about 3 weeks after SOS, followed by a gradual increase to a second peak around 20 weeks after SOS, and then a decrease until the EOS (Figures 5 and 4). Interannual standard deviation was greatest for divergence from about 7 weeks (start of PG) until 20 weeks after SOS, just before mean values decreased.

Increases in functional richness after SOS followed observed changes in the CCI (Figures 5 and 4). A reduction in richness was evident around 15–20 weeks after SOS in 2018, which was also visible in reductions in the pigment-related indices CCI and CIre and, to a lesser extent, in NDMI (Figures 5 and 4). Divergence rapidly increased concurrently with increases in the relative values of all three component indices, but then remained constant in the first 5 weeks after SOS (Figures 5 and 4). A second increase towards a peak or plateau was visible in the later season of every year (Figure 5). The first increase in divergence was earlier in 2019 and 2021 compared to 2017, 2018, and 2020 (Figure 5). The second peak before EOS was more distinct in 2018 and 2020 (Figure 5).

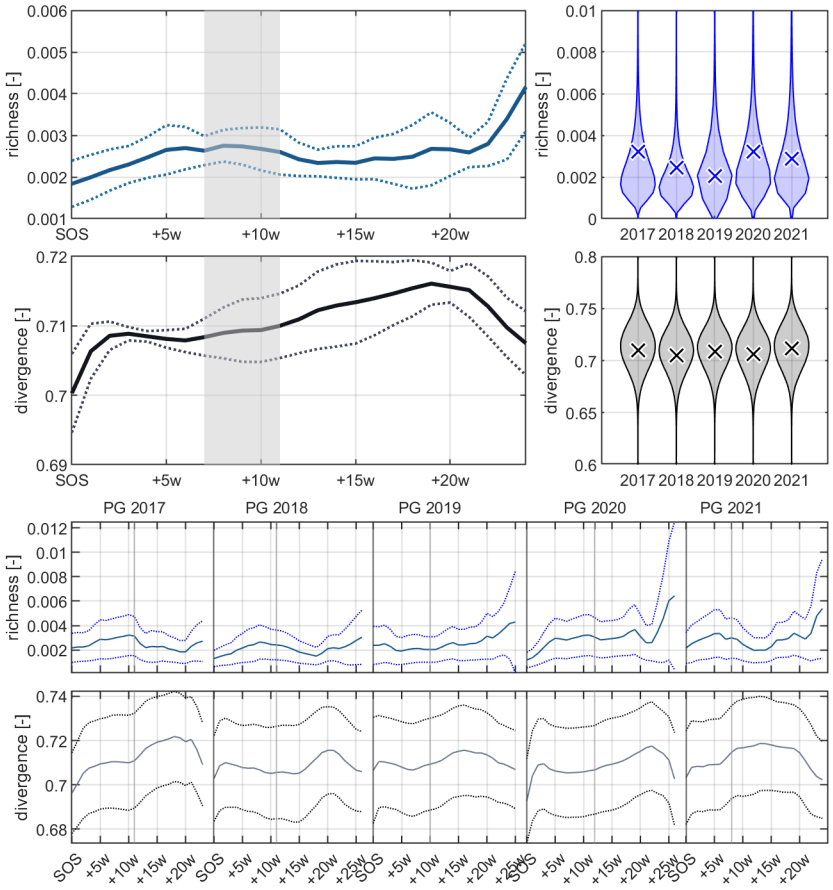

Figure 5: Temporal development of the diversity metrics functional richness (black) and divergence (blue) throughout the growing season. Top left: Time series for the means of these diversity metrics for all years (solid lines) and their respective standard deviations across years (dashed lines), each normalized to SOS. The gray area marks the range of the PG from all years (7–11 weeks after SOS). Top right: Distribution of metric values during the entire growing season of each year for the whole study area as violin plots. Bottom: Temporal development of means of the diversity metrics (solid lines), separate for each year, and the respective standard deviations (dashed lines).

3.4 Comparison of diversity metrics at PG against seasonal curves

Figure 4 helps to determine whether PG is a representative time of the year to measure trait-related indices and diversity across years. The highest values of CIre of a year occurred around PG, while CCI values were at a lower second peak or in-between the highest value and a following trough (2017, 2018, 2021) or directly in a trough (2019, 2020). NDMI values were in a plateau at PG that followed their initial increase immediately after SOS.

In contrast, the values of functional richness and divergence at PG were within a region of relatively little change and thus relatively comparable across the years, following their initial SOS change; however, from year to year, PG did not necessarily capture a similar stage of seasonal dynamics for these diversity metrics (Figure 5). For richness, PG represented a window of relatively low standard deviation across years, although a few weeks later (around 13 weeks following SOS) exhibited lower standard deviation across years. In contrast, for divergence, PG represented a region of relatively high standard deviation across years while a period a few weeks earlier (around 3–5 weeks following SOS) exhibited the lowest standard deviation across years.

3.5 Temporal variation across forest communities

Intra-annual patterns of diversity metrics differed among forest communities (Figure 6). In general, the curve shapes were similar for all forest communities, but with distinct differences in the magnitudes of the maximum and minimum values. Needle tree-dominated stands had higher richness and divergence values compared to the broadleaf tree-dominated stands. *P. abies*-dominated stands had the highest values of richness, and mixed needle leaf-broadleaf stands had values similar to the needle-dominated stands. The divergence curves varied more throughout the year, especially in spring and fall, and divergence patterns of broadleaf species were more stable during PG weeks and delayed compared to the other communities. The highest divergence values of the year were found in mixed stands at around 18–19 weeks after SOS. For richness, the values were mostly the highest at PG (apart from values close to EOS), for divergence, higher values were reached after PG.

The variance components were more stable for divergence between forest communities than for richness (Figure 7). *P. abies*-dominated stands showed the highest variance of divergence across all years. While the spatial and interaction components were high throughout all the communities for divergence, the temporal variation was relatively low, with a bit higher temporal variance for needle tree-dominated stands in 2017 and 2021. For richness, the year 2020 revealed very high variance across all communities, especially for temporal variation. Lastly, we observed a higher temporal and spatial variation in 2020 in *P. abies*-dominated forests for both richness and divergence.

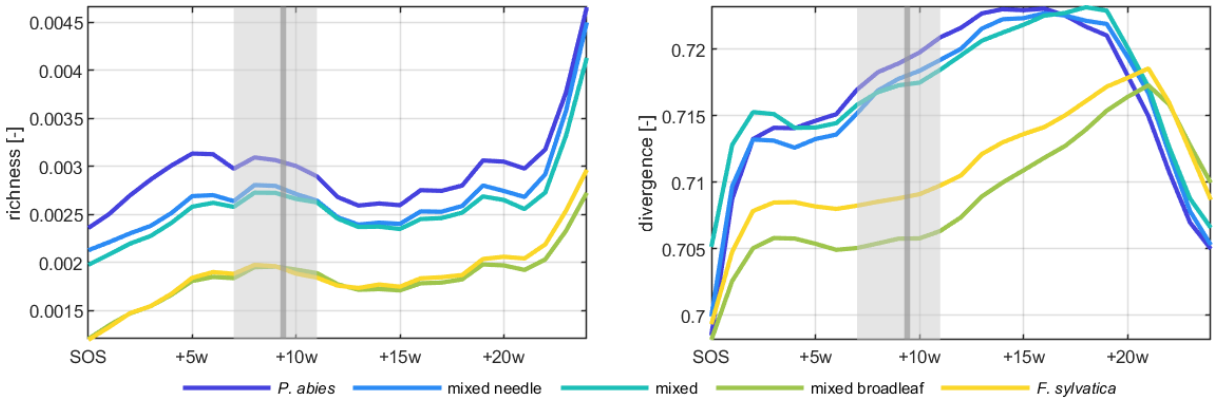

Figure 6: Intra-annual variability of the diversity metrics functional richness (left) and divergence (right) throughout the mean growing season (mean values calculated across all five years) for different forest communities. The gray area marks the range of the PG from all years (7–11 weeks after SOS), and the gray line marks the mean PG date from all five years.

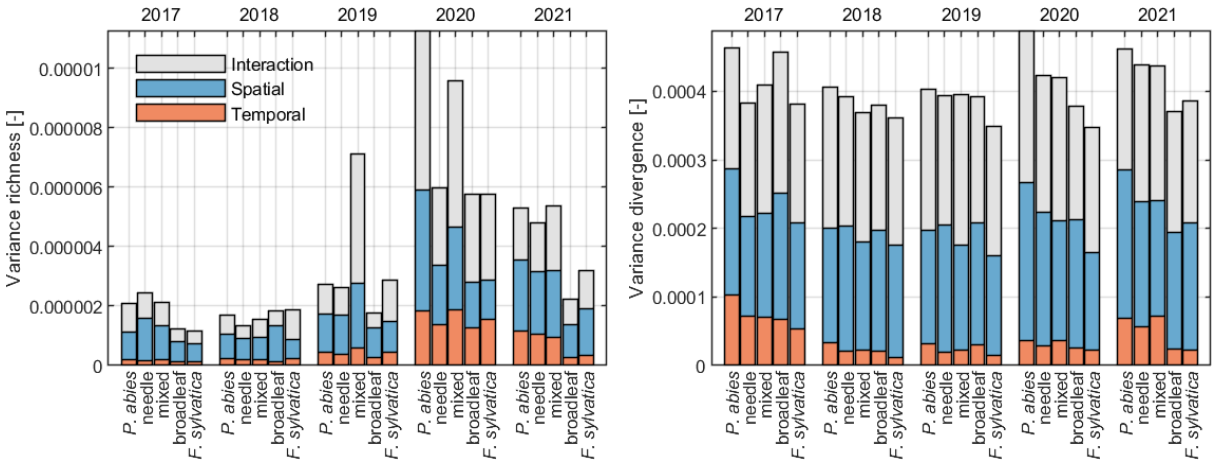

Figure 7: Components of temporal variation (orange), spatial variation (blue) and interaction of both (gray) to the total variation in index-based richness (left) and divergence (right). The variation is analyzed for every year (2017–2021) and for different forest communities (*Picea abies*-dominated, needle-dominated, mixed, broadleaf-dominated, and *Fagus sylvatica*-dominated stands). The calculation is based on the method from Rossi et al. Rossi *et al.* (2021).

4 Discussion

Multi-year, dense time series from satellites such as Sentinel-2 provide unique opportunities to assess forest functional diversity across space and time (Chastain *et al.*, 2019). By analyzing seasonal trajectories of trait-related spectral indices and resulting diversity metrics, we demonstrate how temporal variability shapes assessments of functional richness and divergence across temperate forest communities. Our analysis focuses on a single, well-characterized 30 km × 30 km tile to isolate the effect of acquisition timing and phenological dynamics on functional diversity estimates. This controlled setting avoids confounding variability from climate gradients, species composition, and management history that would complicate temporal interpretations across larger extents, while the results provide a basis for transferring these practices to broader regions. Our results show that diversity estimates derived from satellite observations are strongly dependent on acquisition timing within the growing season.

In particular, we evaluated the representativeness of values at peak greenness (PG) against seasonal curves, highlighting both the potential and the limitations of relying on single-date observations. Additionally, we examined whether diversity metrics have differing temporal dynamics for different forest communities. Our results show intra- and interannual dynamics of spectral index values that vary for different forest communities and target traits, and may be informative of changing environmental conditions. The observed dynamics indicate that it is important to synchronize the collection of *in situ* trait data and remote sensing datasets if one should be used to interpret the other. The most commonly selected observation window in temperate systems, PG, captures different phenological stages for different trait indices, and thus other times of the season should also be considered when designing comparative and time series assessments, depending on the aims that motivate observations.

4.1 Variation of trait-related spectral indices and diversity metrics reveals growing season dynamics

Comparisons of functional diversity across years may yield different results depending on the period in the season at which functional diversity metrics are calculated. The intra-annual analysis of the trait-related indices shows a clear temporal dynamic starting from start of season (SOS). The red-edge chlorophyll index (CIre) and chlorophyll carotenoid index (CCI) first increase, peak at different times, and subsequently decline, reflecting the seasonal cycle of forest vegetation. Importantly, this means the CCI is in decline and thus less consistent during PG. The observed patterns fit the results of trait assessments from imaging spectroscopy in other recent studies (Chlus & Townsend, 2022; Ji *et al.*, 2024). Chlorophyll increase typically suggests active growth, while declines indicate stress-related, seasonal or developmental senescence (Demarez, 1999). CCI is high early in the growing season, indicating that the accumulation of carotenoids precedes the accumulation of chlorophyll in young leaves (Dhami & Cazzonelli, 2020). Later in the growing season, increased CCI, for example, in early July, indicates a response to oxidative stress due

to high light input and potentially water stress (Demmig-Adams & Adams, 1996). We found a small decrease in CCI and CIre at the end of July every year (Figure 4), suggesting a reduction in photosynthesis during this period, which might be linked to summer or midday depression during the timing of the overflight of Sentinel-2 satellites. NDMI shows a maximum early after the SOS, with a plateau followed by a short decline from about 20 weeks after SOS. Although water content trends are expected to reflect precipitation patterns and impact the other two indices, NDMI was mostly stable during the growing season. This might be due to the saturation of NDMI at high leaf area in closed canopies (Jackson *et al.*, 2004).

Increasing functional richness indicates growing index dissimilarity over the season, suggesting a broader range of index values, for example, leaf discoloration before end of season (EOS). In contrast, during times of large-scale stress, such as drought or high-temperature stress, decreasing functional richness is observed. Divergence remains constant at high values before PG and shows a similar trajectory towards the end of the season. Therefore, divergence values are highest after the leaves' initial unfolding and at the onset of leaf senescence, and lowest around PG.

4.2 Interannual variation of trait-related spectral indices and diversity metrics is weather-related

We analyzed the intra-annual mean time series of trait-related indices and diversity metrics, including the standard deviation as a metric for interannual stability (Figures 4 and 5). High variability suggests high sensitivity to seasonal stages or environmental factors, such as weather conditions. In 2018 and 2020, an earlier increase in CIre was detected, contrasting with a delayed SOS in 2019, likely due to a rainy spring (Figure 4 and Table 1). In contrast to strong fluctuations in other years, index variation was lowest in 2019, and NDMI levels were high, which was associated with warm conditions but sufficient water availability.

Low interannual variability indicates consistent, predictable trait expression over the years, while higher variability indicates environmental sensitivity. For example, during PG, CIre showed low variability, indicating similar stages of leaf or needle development (Figure 4). In 2018, CIre stayed high for a longer period of time, while 2020 marked an overall earlier EOS, likely influenced by a cool, wet October (Figure 4 and Table 1). Thus, comparing CIre during PG indicates stability, whereas comparing the development of CIre across these years during each growing season reveals differences concurrent with pronounced environmental differences (Figure 4). Consequently, peak greenness does not necessarily correspond to the same state of functional diversity estimation across years.

Observing within-growing season dynamics may help to better pinpoint specific climate-related events. In 2018, a decrease in CIre and CCI was observed from 15 weeks after SOS (DOY 211, July 30th) (Figure 4). This period coincides with an unusually warm and dry season beginning in April, culminating in a heatwave from the 29th of July to the 6th of August and resulting in a harmful hot summer drought (MeteoSchweiz, 2018). The heatwave's temporal alignment with the observed decline in CIre and CCI suggests a direct impact of extreme heat and drought stress on

vegetation health and pigment concentration. Furthermore, compared to other years, the overall lower water content (as expressed in lower NDMI values) in 2018 reflects the prolonged exposure to dry conditions (MeteoSchweiz, 2018). Further effects of the extreme conditions in 2018 (for weather summary focusing on temperature and precipitation see Table 1) are visible in the pigment-related indices in 2019, as well as in functional richness, which not only decreased in 2018 but was also low in 2019 and recovered in 2020 (Figures 4 and 5). However, as seen in Figure 5, functional richness at PG in 2019 was among the lowest values in that year and somewhat stable. For most years, including 2018, richness at PG was found to be among the higher values of the respective year (Figure 5). A possible explanation for this might be the absence of a richness peak around PG in 2019 compared to the other years, which might be linked to lower CCI around PG. This could be caused by the drought damage of 2018 or the absence of high CCI values in 2019 due to the high water availability and the absence of stress reactions. Data availability might also have caused the absence of the peak in the collected data. Cloud cover and rainfalls hinder data acquisition, which might have caused a potential peak in CCI not to be detected in the 2019 time series. In any case, the result is that when richness values are compared at PG across years, 2019 is rated as having lower richness than 2018, whereas the range of richness values was higher in 2019 than in 2018.

4.3 Implications of peak greenness for annual monitoring

We highlighted the PG values of trait-related indices and diversity metrics to study their variation throughout the growing season. PG occurred between June 21st (2021) and July 7th (2019) (Figure 3). At PG, CIre and NDMI values show relatively little interannual variation, reflecting the choice of maximum greenness values and corresponding stable, higher water content, whereas CCI values were more variable across years, reflecting gradually decreasing CCI values at the end of the leaf unfolding (Figure 4). At PG, richness is at a first peak except for 2019, where this increase in richness was absent (Figure 5). Richness values during PG tended to correspond to different seasonal mean values in richness, but not reliably so, as the PG richness values were sometimes among the highest of that season, and at other times among the lowest (Figure 5). In contrast, divergence at PG was consistently at relatively low values, and differences in divergence across years tracked differences in seasonal means (Figure 5). The timing of the peaks in CCI, NDMI, and divergence varied between years, and a reference close to these peaks might lead to varying results in trait and diversity assessments (Figures 4 and 5).

This implies some considerations when using PG for Sentinel-2-based monitoring of interannual changes in functional diversity. CCI values are decreasing from an earlier peak during PG, and differences in the CCI peak value and the rate of its decline could provide insight into early-season dynamics. In fact, functional divergence was most stable shortly before peak greenness, just after CCI and NDMI values peaked, and just before the peak of CIre, around 3–5 weeks after SOS. Late-season measurements of divergence (around 20 weeks after SOS) were more likely to capture

maximum values and may give insight into late-season dynamics such as impacts of droughts (Brun *et al.*, 2020). In contrast, functional richness values were most stable at 5–15 weeks after SOS, a period stretching before, during, and after PG. This suggests that a timepoint shortly before the onset of PG at about 5 weeks SOS could capture the most similar values of functional richness and divergence across years in our study area. Such phenology-aligned observation windows may therefore provide more robust diversity estimates than a single reference date. However, by investigating differences within and between growing seasons, we also identify time series features, similar to phenometrics in land surface phenology (LSP) (Garonna *et al.*, 2016), which may yield more insight into trait dynamics. Overall, our results show that observations during PG are generally associated with stable and high CIre and NDMI, providing a consistent baseline for annual monitoring of these indices and potentially their related traits of chlorophyll and water content, but observations about 2 weeks before PG yield more stable values of functional richness and divergence when including CCI as a third trait-related index. These specific timing windows are derived from this single temperate study area and should be treated as context-dependent. However, they demonstrate that choosing an alternative reference time window for interannual monitoring can meaningfully affect results in mapping and monitoring functional diversity metrics. The optimal observation window depends on the target variable. PG remains a suitable time for CIre and NDMI as standalone indices, but for combined index-based diversity metrics, a window approximately 5 weeks after SOS provides more stable interannual comparisons in our temperate study area.

4.4 Diversity metric variability across different forest communities

We found higher values of richness and divergence in needle tree-dominated stands compared to broadleaf-dominated stands, consistent with previous findings (Helfenstein *et al.*, 2022). Recent observations indicate that these higher values might result in part from shaded areas in these forest types, especially later in the season, due to the more heterogeneous shape of the canopy (Kesselring *et al.*, 2024). Thus, in interpreting our results and applying this approach, it is important to keep in mind that the functional diversity metrics are derived from three specific trait-related indices and that, as with any method, there are inherent biases in our observations. Nevertheless, a recent study using this approach to measure functional diversity identified positive or hump-shaped relationships of diversity with forest drought responses, similar to relationships documented in forest diversity experiments and using additional indices (Schneider *et al.*, 2023; Zheng *et al.*, 2023; Helfenstein *et al.*, 2025). The highest divergence was observed in late summer in mixed and needle tree-dominated stands. On the other hand, in broad-leaf stands, a higher relative peak in divergence around 20 weeks after SOS might be linked to leaf coloration in fall. These differences highlight that both canopy composition and seasonal dynamics influence the interpretation of remotely sensed diversity metrics.

The variance components (spatial, temporal and interaction of both) in Figure 7 revealed more stable conditions for divergence than for richness in forest communities. We observed low variance in 2017 and 2018, higher total variance of richness and divergence, after the drought year, especially in *P. abies* in 2020 and 2021. This observation might indicate time-lagged drought response effects visible in additional physiological changes or secondary drought effects especially affecting *P. abies* in those years, such as dieback and pests, like bark beetle outbreaks (Stroheker *et al.*, 2020). During the 2019 growing season, we observed a greater spatial and interaction variance for richness in mixed forests, which could indicate different reactions to the summer drought of the previous year through different types of mixed forests.

We observed a higher and more stable variance for divergence than for richness, which could be correlated with the calculation method. Divergence is calculated as a ratio of Euclidean distances, while alpha-shapes used to calculate richness may be more buffered against extreme values (Gruson, 2020). Overall, we found the lowest variance of divergence in broadleaf and *F. sylvatica*-dominated forests, especially in the temporal domain relating to the uniform temporal onset of senescence on the community scale. This observation fits the clear peak of divergence in the seasonal variability of broadleaf-dominated forest stands (Figure 6).

4.5 Validation of trait-related indices and diversity metrics in multitemporal satellite datasets and multi-year, dense time series

Remote sensing platforms with high spatial coverage and frequent revisit times, such as Sentinel-2, allow the derivation of dense multitemporal data streams. Here, we analysed the variation in spectral indices in time and space as a basis for index-based diversity metrics. These multispectral indices were designed as proxies for canopy traits, but their values are affected by changes in multiple traits (Grubinger *et al.*, 2025). We are therefore careful not to ascribe direct meaning to these indices without physiological measurements to support them. Instead, we aim to interpret patterns in these commonly used spectral indices, and indicate possible physiological interpretations based on the original design (Grubinger *et al.*, 2025) and previous validation of these indices (Ali *et al.*, 2020; Gamon *et al.*, 2016; Wong *et al.*, 2020; Guzmán Q. *et al.*, 2023; Sturm *et al.*, 2022; Bloom *et al.*, 2025), and evaluate how these influence functional diversity metrics over seasonal and multiannual time scales. Field-based trait and diversity measurements collected with corresponding spatial and temporal extent and resolution could strengthen the interpretation of these indices.

Trait validation is affected by variability in canopy reflectance, signals of non-forest material in forest gaps and the atmosphere, changing illumination and viewing geometries and the effect of shaded areas in the canopy (Cavender-Bares *et al.*, 2017), and other challenges when downscaling to leaf traits from the measurements at canopy level (Homolová *et al.*, 2013; Malenovský *et al.*, 2019). The mismatch between *in situ* ecological sampling units such as

leaves per canopy, usually sampled in randomized distributed designs, and the generally much coarser and yet, continuous grid of satellite remote sensing raster products complicates comparisons of these data types and thus the ecological interpretation of satellite remote sensing data (Wang & Gamon, 2019; Hauser *et al.*, 2021). Trait observations are typically made *in situ* only once or at most a few times per season. There are large temporal mismatches between most available *in situ* and satellite data (Chavana-Bryant *et al.*, 2017). Current datasets cannot capture the full temporal dynamics needed for the rigorous validation of such dense time series spanning multiple years, and the generation of truly representative canopy trait data on a weekly basis for a 30 km^2 tile represents an unprecedented and very expensive *in situ* sampling and sample analysis effort. Challenges in validating temporally dense and spatially continuous remote-sensing time series remains a major limitation for functional diversity assessments. Neither global trait products nor existing field campaigns provide trait measurements at the temporal frequency of Sentinel-2, making it difficult to evaluate seasonal trajectories of trait-related indices.

Recent studies using multitemporal satellite data propose partial strategies to address this gap. Mederer *et al.* (2025) use a model-based trait framework and internal temporal consistency checks across hyperspectral scenes using EnMap data, while (Liu *et al.*, 2025) employ field-based species diversity measurements to validate multi-temporal spectral diversity metrics from Sentinel-2 and PlanetScope data. These approaches demonstrate feasible pathways for linking remotely-sensed diversity measures to ecological information collected on the ground, but are neither spatially continuous nor seasonally resolved.

Unlike these studies, our work provides dense, multi-year Sentinel-2 time series at a consistent spatial location, allowing us to quantify intra- and interannual trajectories of trait-related indices and their effects on functional diversity in relation to the ecosystem's phenology. Our method builds on existing validation and upscaling work that established the suitability of CIre, CCI, and NDMI for temperate forests (Schneider *et al.*, 2014, 2017; Helfenstein *et al.*, 2022) and demonstrated their ecological relevance through links to ecosystem functioning (Helfenstein *et al.*, 2025). Here, we quantify the temporal behavior of these indices and examine how seasonal and interannual dynamics propagate into calculations of functional richness and divergence across forest communities. The observed patterns indicate the need for coordinated, temporally resolved field campaigns capable of capturing intra-seasonal variation in canopy traits to support ecological interpretations. Developing such datasets will be essential to validate interpretations of functional diversity time series and to advance trait-based biodiversity assessments at the landscape and regional scale.

4.6 Towards monitoring functional diversity using satellite data

There is a need to monitor biodiversity and observe temporal changes to quantify diversity change and predict its consequences, including biodiversity loss as well as the impacts of biodiversity protection and restoration efforts.

There are many challenges that must be met to achieve a systematic approach to biodiversity assessment and monitoring (Gonzalez *et al.*, 2023). Remote sensing can complement *in situ* observations by providing information on diversity and ecosystem processes at regional to global scales and in cases where sufficient ground data are missing. Using multi-year, dense satellite time series for monitoring approaches has great potential to fill current gaps in the coverage of biodiversity monitoring systems (Schmeller *et al.*, 2017). Although functional diversity metrics derived from spectral indices are not yet standard in biodiversity monitoring programs, they provide an interpretable and computationally accessible approach for establishing best practices in remote sensing-based biodiversity monitoring that may transfer to other metrics and regions.

We found that it is essential to align time series to SOS to enable comparisons across years, meaning that not the date as such is relevant for monitoring, but the phenological state of vegetation. This is likely an important consideration for the comparison of any indicators that rely on the state of vegetation or vegetation indices. From the yearly time series, individual characteristics and their temporal occurrence can be derived, e.g., when comparing the time of maximum value of an index or diversity metric, which could already be used as a metric for monitoring. However, such parameters are best assessed using dense time series, which is currently only available from revisiting satellite missions. Instead of data- and processing-intensive time series approaches, efforts to identify SOS and PG could be complemented by *in-situ* observation of phenological stages, e.g., from phenological networks such as Phaenonet (MeteoSchweiz, 2020b). Based on these *in situ* phenological observations, PG or other time window adjustments could support the planning of field measurement of diversity measures, such as traits, or additional remote-sensing-based systems, such as drone or airplane overflights, or support near-real-time monitoring of diversity.

During PG, acquisitions can be combined into composites to fill gaps due to local cloud coverage or illumination issues, leading to large variability between single images. Single cloud-free images are rare because of the variability of clouds and cloud shadows, which can be mitigated by using composites that cover multiple points in time. The variation of PG of up to 16 days in our study emphasized the importance of identifying PG or the other relevant phenological stages, and of defining a broad enough time window for mapping trait diversity. The difference in PG timings will increase further when monitoring larger areas or longer time spans, and hence, this identification is paramount. In the present study area, a June/July composite should cover the observed PG variation. However, this might not be true for other regions of the world, or in long time series. This time window might have changed similarly to the timing of bud-burst in the last decades due to climate warming (Fu *et al.*, 2014), and it is not clear how the changing climate will affect the timing in future climate scenarios (Wenden *et al.*, 2020).

While spectral bandwidth was shown to have a minor role in index retrieval (Helfenstein *et al.*, 2022), an increased number of spectral bands allows for more possibilities in deriving canopy trait-related information. A higher spectral resolution will likely enable the retrieval of additional indices, such as indices indicative of cellulose content (Nagler

et al., 2003). New spaceborne imaging spectrometers, such as the operational EnMap (Guanter *et al.*, 2015) or future missions such as CHIME (Rast *et al.*, 2021) will, therefore, enable new possibilities in spaceborne diversity monitoring. However, many new space-based imaging spectrometers do not share the high temporal resolution of Sentinel-2, which might limit the potential of these systems. Scientific missions such as EnMap do not have a fixed revisit time for collecting imagery unless specific observations are requested and scheduled by users (Heiden *et al.*, 2010). Future operational missions, such as CHIME, plan for a temporal resolution of less than 10 days using two satellites (Buschkamp *et al.*, 2023). The temporal resolution crucial for dense time series approaches could be improved by using multisensor approaches, e.g., by combining Sentinel-2 with other spaceborne missions such as Landsat (Weber *et al.*, 2023) or Landsat 8 with SAR data, e.g., from Sentinel-1 (Shimizu *et al.*, 2019), depending on the target of interest. It is important to keep in mind that the lower native spatial resolution of different sensors might further limit mapping and monitoring efforts, as the resolution of the index data is of primary importance to interpreting results (Helfenstein *et al.*, 2022; Pacheco-Labrador *et al.*, 2022). Finally, such new capacities to calculate functional diversity from space will require investigations such as this and a previous study to determine the effects of spatiotemporal scale and derive guidelines for best practices (Helfenstein *et al.*, 2022).

Our study contributes to identifying stable periods that provide a reliable baseline for detecting significant environmental changes and calibrating remote sensing models for ecological monitoring. Our results indicate that remotely sensed trait-related diversity assessment should not always be conducted at PG, and that the temporal dynamics of the signal may be important for its interpretation. This cannot only inform when it is best to conduct *in situ* measurements for different assessment and monitoring purposes, but also demonstrates the high value of using multi-year, dense satellite time series to complement monitoring efforts.

5 Conclusion

Multi-year, dense time series from satellites with short revisit intervals enable monitoring of the temporal dynamics of trait-related spectral indices and associated diversity metrics in forest ecosystems. Their high spatiotemporal coverage complements *in situ* and drone-based approaches, providing a broader perspective on ecosystem functioning.

Using Sentinel-2 data from 2017–2021, we showed that spectral indices linked to chlorophyll, carotenoids, and water content, as well as derived functional richness and divergence, exhibit pronounced seasonal and interannual variability. Our results highlight that relying solely on one date around peak greenness limits the information content and interpretability of remotely sensed diversity estimates. Broader temporal windows are therefore likely necessary to capture ecosystem responses to environmental stressors and to assess resilience. We furthermore found systematic

differences among forest communities, with higher diversity values in needle-dominated stands, and observed that functional divergence is more stable across space and time than richness.

These findings emphasize the importance of accounting for temporal dynamics in biodiversity assessment and monitoring, and demonstrate how Sentinel-2 can support time-resolved, multi-annual observations of forest functional diversity. Incorporating such temporal perspectives may improve the accuracy of ecosystem assessments. The resulting time-resolved diversity estimates, derived from computationally simple indices and public data, have potential to guide conservation and management strategies under changing environmental conditions.

Acknowledgements

This research project and related results were made possible with the support of the NOMIS Foundation grant Remotely Sensing Ecological Genomics and the University Research Priority Program on Global Change and Biodiversity of the University of Zurich. The work of T. L. Koch was supported by the Swiss National Science Foundation (SNSF) (grant number 200021_184605).

6 References

Ali AM, Darvishzadeh R, Skidmore A, *et al.* (2020) Comparing methods for mapping canopy chlorophyll content in a mixed mountain forest using Sentinel-2 data. *International Journal of Applied Earth Observation and Geoinformation*, **87**, 102037.

Baudirektion Kanton Zürich (2020) Zwischenbericht Waldentwicklung 2020. Tech. rep., Zürich.

Blickensdörfer L, Oehmichen K, Pflugmacher D, Kleinschmit B, Hostert P (2024) National tree species mapping using Sentinel-1/2 time series and German National Forest Inventory data. *Remote Sensing of Environment*, **304**, 114069.

Bloom CK, Koch TL, Meusburger K, *et al.* (2025) Towards near real-time drought stress assessment in Europe's temperate forests – comparing remote sensing time series with continuous in-situ tree-level measurements. *Ecological Indicators*, **177**, 113757.

Broich M, Huete A, Tulbure MG, *et al.* (2014) Land surface phenological response to decadal climate variability across Australia using satellite remote sensing. *Biogeosciences*, **11**, 5181–5198.

Brun P, Psomas A, Ginzler C, Thuiller W, Zappa M, Zimmermann NE (2020) Large-scale early-wilting response of Central European forests to the 2018 extreme drought. *Global Change Biology*, **26**, 7021–7035.

Buermann W, Forkel M, O'Sullivan M, *et al.* (2018) Widespread seasonal compensation effects of spring warming on northern plant productivity. *Nature*, **562**, 110–114.

Bürgi M, Schuler A (2003) Driving forces of forest management—an analysis of regeneration practices in the forests of the Swiss Central Plateau during the 19th and 20th century. *Forest Ecology and Management*, **176**, 173–183.

Buschkamp P, Hofmann J, Rio-Fernandes D, *et al.* (2023) CHIME's Hyperspectral Imager (HSI): Status of instrument design and performance at PDR. *International Conference on Space Optics — ICSO 2022*, **12777**, 1277737–1277737–20.

Cavender-Bares J, Gamon JA, Hobbie SE, Madritch MD, Meireles JE, Schweiger AK, Townsend PA (2017) Harnessing plant spectra to integrate the biodiversity sciences across biological and spatial scales. *American Journal of Botany*, **104**, 966–969.

Chastain R, Housman I, Goldstein J, Finco M, Tenneson K (2019) Empirical cross sensor comparison of Sentinel-2A and 2B MSI, Landsat-8 OLI, and Landsat-7 ETM+ top of atmosphere spectral characteristics over the conterminous United States. *Remote Sensing of Environment*, **221**, 274–285.

Chavana-Bryant C, Malhi Y, Wu J, *et al.* (2017) Leaf aging of Amazonian canopy trees as revealed by spectral and physiochemical measurements. *New Phytologist*, **214**, 1049–1063.

Chlus A, Townsend PA (2022) Characterizing seasonal variation in foliar biochemistry with airborne imaging spectroscopy. *Remote Sensing of Environment*, **275**, 113023.

Cornelissen JHC, Lavorel S, Garnier E, *et al.* (2003) A handbook of protocols for standardised and easy measurement of plant functional traits worldwide. *Australian Journal of Botany*, **51**, 335–380.

Da R, Hao M, Qiao X, Zhang C, Zhao X (2022) Unravelling Trait–Environment Relationships at Local and Regional Scales in Temperate Forests. *Frontiers in Plant Science*, **13**, 907839.

Delegido J, Verrelst J, Alonso L, Moreno J (2011) Evaluation of Sentinel-2 Red-Edge Bands for Empirical Estimation of Green LAI and Chlorophyll Content. *Sensors*, **11**, 7063–7081.

Demarez V (1999) Seasonal variation of leaf chlorophyll content of a temperate forest. Inversion of the PROSPECT model. *International Journal of Remote Sensing*, **20**, 879–894.

Demmig-Adams B, Adams WW (1996) The role of xanthophyll cycle carotenoids in the protection of photosynthesis. *Trends in Plant Science*, **1**, 21–26.

Dhami N, Cazzonelli CI (2020) Environmental impacts on carotenoid metabolism in leaves. *Plant Growth Regulation*, **92**, 455–477.

Fassnacht FE, Müllerová J, Conti L, Malavasi M, Schmidtlein S (2022) About the link between biodiversity and spectral variation. *Applied Vegetation Science*, **25**, e12643.

Forkel M, Carvalhais N, Verbesselt J, Mahecha MD, Neigh CS, Reichstein M (2013) Trend Change Detection in NDVI Time Series: Effects of Inter-Annual Variability and Methodology. *Remote Sensing*, **5**, 2113–2144.

Frantz D (2019) FORCE—Landsat + Sentinel-2 Analysis Ready Data and Beyond. *Remote Sensing*, **11**, 1124.

Frantz D, Haß E, Uhl A, Stoffels J, Hill J (2018) Improvement of the Fmask algorithm for Sentinel-2 images: Separating clouds from bright surfaces based on parallax effects. *Remote Sensing of Environment*, **215**, 471–481.

Fu YH, Piao S, de Beeck MO, *et al.* (2014) Recent spring phenology shifts in western Central Europe based on multiscale observations. *Global Ecology and Biogeography*, **23**, 1255–1263.

Gamon JA, Huemmrich KF, Wong CYS, *et al.* (2016) A remotely sensed pigment index reveals photosynthetic phenology in evergreen conifers. *Proceedings of the National Academy of Sciences*, **113**, 13087–13092.

Gao BC (1996) NDWI—A normalized difference water index for remote sensing of vegetation liquid water from space. *Remote Sensing of Environment*, **58**, 257–266.

Garonna I, de Jong R, Stöckli R, Schmid B, Schenkel D, Schimel D, Schaepman ME (2018) Shifting relative importance of climatic constraints on land surface phenology. *Environmental Research Letters*, **13**, 024025.

Garonna I, Jong R, Schaepman ME (2016) Variability and evolution of global land surface phenology over the past three decades (1982–2012). *Global Change Biology*, **22**, 1456–1468.

Garonna I, Jong R, Wit AJ, Mücher CA, Schmid B, Schaepman ME (2014) Strong contribution of autumn phenology to changes in satellite-derived growing season length estimates across Europe (1982–2011). *Global Change Biology*, **20**, 3457–3470.

Gazol A, Camarero JJ (2016) Functional diversity enhances silver fir growth resilience to an extreme drought. *Journal of Ecology*, **104**, 1063–1075.

GIS-ZH (2019) Waldareal (OGD).

GIS-ZH (2023) Luftbild-Bestandeskarte (OGD).

Gitelson AA, Gritz Y, Merzlyak MN (2003) Relationships between leaf chlorophyll content and spectral reflectance and algorithms for non-destructive chlorophyll assessment in higher plant leaves. *Journal of Plant Physiology*, **160**, 271–282.

Gonzalez A, Vihervaara P, Balvanera P, *et al.* (2023) A global biodiversity observing system to unite monitoring and guide action. *Nature Ecology & Evolution*, **7**, 1947–1952.

Grubinger S, Coops NC, O'Neill GA, *et al.* (2025) Seasonal vegetation dynamics for phenotyping using multispectral drone imagery: Genetic differentiation, climate adaptation, and hybridization in a common-garden trial of interior spruce (Picea engelmannii × glauca). *Remote Sensing of Environment*, **317**, 114512.

Gruson H (2020) Estimation of colour volumes as concave hypervolumes using alpha-shapes. *Methods in Ecology and Evolution*, **11**, 955–963.

Guanter L, Kaufmann H, Segl K, *et al.* (2015) The EnMAP Spaceborne Imaging Spectroscopy Mission for Earth Observation. *Remote Sensing*, **7**, 8830–8857.

Guzmán Q JA, Pinto-Ledezma JN, Frantz D, Townsend PA, Juzwik J, Cavender-Bares J (2023) Mapping oak wilt disease from space using land surface phenology. *Remote Sensing of Environment*, **298**, 113794.

Hauser LT, Féret JB, Binh NA, *et al.* (2021) Towards scalable estimation of plant functional diversity from Sentinel-2: In-situ validation in a heterogeneous (semi-)natural landscape. *Remote Sensing of Environment*, **262**, 112505.

Hauser LT, Timmermans J, Soudzilovskaia NA, van Bodegom PM (2022) Linking Land Use and Plant Functional Diversity Patterns in Sabah, Borneo, through Large-Scale Spatially Continuous Sentinel-2 Inference. *Land*, **11**, 572.

Heiden U, Gredel J, Pinnel N, *et al.* (2010) The user interface of the EnMap satellite mission. *2010 IEEE International Geoscience and Remote Sensing Symposium*, pp. 4268–4271.

Helfenstein IS, Schneider FD, Schaepman ME, Morsdorf F (2022) Assessing biodiversity from space: Impact of spatial and spectral resolution on trait-based functional diversity. *Remote Sensing of Environment*, **275**, 113024.

Helfenstein IS, Sturm JT, Schmid B, Damm A, Schuman MC, Morsdorf F (2025) Satellite Observations Reveal a Positive Relationship Between Trait-Based Diversity and Drought Response in Temperate Forests. *Global Change Biology*, **31**, e70059.

Hmimina G, Dufrêne E, Pontailler JY, *et al.* (2013) Evaluation of the potential of MODIS satellite data to predict vegetation phenology in different biomes: An investigation using ground-based NDVI measurements. *Remote Sensing of Environment*, **132**, 145–158.

Homolová L, Malenovský Z, Clevers JG, García-Santos G, Schaepman ME (2013) Review of optical-based remote sensing for plant trait mapping. *Ecological Complexity*, **15**, 1–16.

Hordijk I, Poorter L, Liang J, *et al.* (2025) Effect of climate on traits of dominant and rare tree species in the world's forests. *Nature Communications*, **16**, 4773.

Huang L, Xue W, Herben T (2019) Temporal niche differentiation among species changes with habitat productivity and light conditions. *Journal of Vegetation Science*, **30**, 438–447.

Huemmrich KF, Black TA, Jarvis PG, McCaughey JH, Hall FG (1999) High temporal resolution NDVI phenology from micrometeorological radiation sensors. *Journal of Geophysical Research: Atmospheres*, **104**, 27935–27944.

Immitzer M, Vuolo F, Atzberger C (2016) First Experience with Sentinel-2 Data for Crop and Tree Species Classifications in Central Europe. *Remote Sensing*, **8**, 166.

Jackson TJ, Chen D, Cosh M, *et al.* (2004) Vegetation water content mapping using Landsat data derived normalized difference water index for corn and soybeans. *Remote Sensing of Environment*, **92**, 475–482.

Jetz W, Cavender-Bares J, Pavlick R, *et al.* (2016) Monitoring plant functional diversity from space. *Nature Plants*, **2**, 16024.

Ji F, Li F, Hao D, *et al.* (2024) Unveiling the transferability of PLSR models for leaf trait estimation: Lessons from a comprehensive analysis with a novel global dataset. *New Phytologist*, **243**, 111–131.

Kesselring J, Morsdorf F, Kükenbrink D, Gastellu-Etchegorry JP, Damm A (2024) Diversity of 3D APAR and LAI dynamics in broadleaf and coniferous forests: Implications for the interpretation of remote sensing-based products. *Remote Sensing of Environment*, **306**, 114116.

Koch TL, Grubinger S, Coops NC, *et al.* (2025a) Assessment of tree species specific phenology metrics from Sentinel-2 data to complement in situ monitoring. *Ecological Indicators*, **180**, 114299.

Koch TL, Hobi ML, Morsdorf F, *et al.* (2025b) Assessing Intraspecific Variation of Tree Species Based on Sentinel-2 Vegetation Indices Across Space and Time. *REMOTE SENSING*, **17**.

Koch TL, Weber D, Waser L (2024) Sentinel-2 imagery of Switzerland.

Lang N, Schindler K, Wegner JD (2019) Country-wide high-resolution vegetation height mapping with Sentinel-2. *Remote Sensing of Environment*, **233**, 111347.

Lara B, Gandini M (2016) Assessing the performance of smoothing functions to estimate land surface phenology on temperate grassland. *International Journal of Remote Sensing*, **37**, 1801–1813.

Laureto LMO, Cianciaruso MV, Samia DSM (2015) Functional diversity: An overview of its history and applicability. *Natureza e Conservacao*, **13**, 112—116.

Lindenmayer DB, Westgate MJ, Scheele BC, Foster CN, Blair DP (2019) Key perspectives on early successional forests subject to stand-replacing disturbances. *Forest Ecology and Management*, **454**, 117656.

Liu J, Wang Z, Sun Z, *et al.* (2025) Integrating multi-temporal information for monitoring plant spectral diversity with PlanetScope and Sentinel-2 satellite imagery. *Ecological Indicators*, **180**, 114348.

Malenovský Z, Homolová L, Lukeš P, *et al.* (2019) Variability and Uncertainty Challenges in Scaling Imaging Spectroscopy Retrievals and Validations from Leaves Up to Vegetation Canopies. *Surveys in Geophysics*, **40**, 631–656.

Mason NWH, Mouillot D, Lee WG, Wilson JB (2005) Functional richness, functional evenness and functional divergence: The primary components of functional diversity. *Oikos*, **111**, 112–118.

Maynard DS, Bialic-Murphy L, Zohner CM, *et al.* (2022) Global relationships in tree functional traits. *Nature Communications*, **13**, 3185.

Mederer D, Kattenborn T, Cherif E, Guimaraes-Steinicke C, Joswig JS, Schneider FD, Feilhauer H (2025) Unraveling the seasonality of functional diversity through remote sensing. *Communications Earth & Environment*, **6**, 790.

MeteoSchweiz (2018) Klimabulletin Jahr 2017. Tech. rep., Bundesamt für Meteorologie und Klimatologie MeteoSchweiz.

MeteoSchweiz (2019) Klimabulletin Jahr 2018. Tech. rep., Bundesamt für Meteorologie und Klimatologie MeteoSchweiz.

MeteoSchweiz (2020a) Klimabulletin Jahr 2019. Tech. rep., Bundesamt für Meteorologie und Klimatologie MeteoSchweiz.

MeteoSchweiz (2020b) Phenophasen 2020 Oberehrendingen: Darstellung der Resultate auf PhaenoNet. Tech. rep.

MeteoSchweiz (2021) Klimabulletin Jahr 2020. Tech. rep., Bundesamt für Meteorologie und Klimatologie MeteoSchweiz.

MeteoSchweiz (2022) Klimabulletin Sommer 2022. Tech. rep., Bundesamt für Meteorologie und Klimatologie MeteoSchweiz.

Morellato LPC, Alberton B, Alvarado ST, *et al.* (2016) Linking plant phenology to conservation biology. *Biological Conservation*, **195**, 60–72.

Nagler PL, Inoue Y, Glenn EP, Russ AL, Daughtry CST (2003) Cellulose absorption index (CAI) to quantify mixed soil-plant litter scenes. *Remote Sensing of Environment*, **87**, 310–325.

O'Connor B, Bojinski S, Röösli C, Schaepman ME (2020) Monitoring global changes in biodiversity and climate essential as ecological crisis intensifies. *Ecological Informatics*, **55**, 101033.

Pacheco-Labrador J, Migliavacca M, Ma X, *et al.* (2022) Challenging the link between functional and spectral diversity with radiative transfer modeling and data. *Remote Sensing of Environment*, **280**, 113170.

Pan H, Chen Z, Ren J, Li H, Wu S (2018) Modeling Winter Wheat Leaf Area Index and Canopy Water Content With Three Different Approaches Using Sentinel-2 Multispectral Instrument Data. *IEEE Journal of Selected Topics in Applied Earth Observations and Remote Sensing*, **12**, 482–492.

Phiri D, Simwanda M, Salekin S, Nyirenda VR, Murayama Y, Ranagalage M (2020) Sentinel-2 Data for Land Cover/Use Mapping: A Review. *Remote Sensing*, **12**, 2291.

Rast M, Nieke J, Adams J, Isola C, Gascon F (2021) Copernicus Hyperspectral Imaging Mission for the Environment (CHIME). *2021 IEEE International Geoscience and Remote Sensing Symposium IGARSS*, pp. 108–111.

Rengarajan R, Choate M, Storey J, Franks S, Micijevic E (2020) Landsat Collection-2 geometric calibration updates. *Earth Observing Systems XXV*, **11501**, 115010N–115010N–11.

Revermann R, Finckh M, Stellmes M, Strohbach BJ, Frantz D, Oldeland J (2016) Linking Land Surface Phenology and Vegetation-Plot Databases to Model Terrestrial Plant alpha-Diversity of the Okavango Basin. *Remote Sensing*, **8**, 370.

Rodríguez-Ezpeleta N, Zinger L, Kinziger A, *et al.* (2021) Biodiversity monitoring using environmental DNA. *Molecular Ecology Resources*, **21**, 1405–1409.

Rosenzweig C, Karoly D, Vicarelli M, *et al.* (2008) Attributing physical and biological impacts to anthropogenic climate change. *Nature*, **453**, 353–357.

Rossi C, Kneubühler M, Schütz M, Schaepman ME, Haller RM, Risch AC (2020) From local to regional: Functional diversity in differently managed alpine grasslands. *Remote Sensing of Environment*, **236**, 111415.

Rossi C, Kneubühler M, Schütz M, Schaepman ME, Haller RM, Risch AC (2021) Remote sensing of spectral diversity: A new methodological approach to account for spatio-temporal dissimilarities between plant communities. *Ecological Indicators*, **130**, 108106.

Rüetschi M, Weber D, Koch TL, Waser LT, Small D, Ginzler C (2021) Countrywide mapping of shrub forest using multi-sensor data and bias correction techniques. *International Journal of Applied Earth Observation and Geoinformation*, **105**, 102613.

Rufin P, Frantz D, Yan L, Hostert P (2021) Operational Coregistration of the Sentinel-2A/B Image Archive Using Multitemporal Landsat Spectral Averages. *IEEE Geoscience and Remote Sensing Letters*, **18**, 712–716.

Scherrer D, Baltensweiler A, Bürgi M, Fischer C, Stadelmann G, Wohlgemuth T (2023) Low naturalness of Swiss broadleaf forests increases their susceptibility to disturbances. *Forest Ecology and Management*, **532**, 120827.

Schmeller DS (2008) European species and habitat monitoring: Where are we now? *Biodiversity and Conservation*, **17**, 3321–3326.

Schmeller DS, Böhm M, Arvanitidis C, *et al.* (2017) Building capacity in biodiversity monitoring at the global scale. *Biodiversity and Conservation*, **26**, 2765–2790.

Schneider FD, Leiterer R, Morsdorf F, Gastellu-Etchegorry JP, Lauret N, Pfeifer N, Schaepman ME (2014) Simulating imaging spectrometer data: 3D forest modeling based on LiDAR and in situ data. *Remote Sensing of Environment*, **152**, 235–250.

Schneider FD, Longo M, Paul-Limoges E, *et al.* (2023) Remote Sensing-Based Forest Modeling Reveals Positive Effects of Functional Diversity on Productivity at Local Spatial Scale. *JOURNAL OF GEOPHYSICAL RESEARCH-BIOGEOSCIENCES*, **128**.

Schneider FD, Morsdorf F, Schmid B, Petchey OL, Hueni A, Schimel DS, Schaepman ME (2017) Mapping functional diversity from remotely sensed morphological and physiological forest traits. *Nature Communications*, **8**, 1441.

Schuldt B, Buras A, Arend M, *et al.* (2020) A first assessment of the impact of the extreme 2018 summer drought on Central European forests. *Basic and Applied Ecology*, **45**, 86–103.

Schwieder M, Leitão PJ, Bustamante MMdC, Ferreira LG, Rabe A, Hostert P (2016) Mapping Brazilian savanna vegetation gradients with Landsat time series. *International Journal of Applied Earth Observation and Geoinformation*, **52**, 361–370.

Segarra J, Buchaillot ML, Araus JL, Kefauver SC (2020) Remote Sensing for Precision Agriculture: Sentinel-2 Improved Features and Applications. *Agronomy*, **10**, 641.

Shimizu K, Ota T, Mizoue N (2019) Detecting Forest Changes Using Dense Landsat 8 and Sentinel-1 Time Series Data in Tropical Seasonal Forests. *Remote Sensing*, **11**, 1899.

Skidmore AK, Coops NC, Neinavaz E, *et al.* (2021) Priority list of biodiversity metrics to observe from space. *Nature Ecology & Evolution*, **5**, 896–906.

Soudani K, Hmimina G, Delpierre N, *et al.* (2012) Ground-based Network of NDVI measurements for tracking temporal dynamics of canopy structure and vegetation phenology in different biomes. *Remote Sensing of Environment*, **123**, 234–245.

Springer K, Wang R, Gamon J (2017) Parallel Seasonal Patterns of Photosynthesis, Fluorescence, and Reflectance Indices in Boreal Trees. *Remote Sensing*, **9**, 691.

Stroheker S, Forster B, Queloz V (2020) Zweithöchster je registrierter Buchdruckerbefall (Ips typographus) in der Schweiz. *Waldschutz aktuell*, **1/2020**, 2.

Sturm J, Santos MJ, Schmid B, Damm A (2022) Satellite data reveal differential responses of Swiss forests to unprecedented 2018 drought. *Global Change Biology*, **28**, 2956–2978.

swisstopo (2021) swissBOUNDARIES3D.

Torresani M, Rocchini D, Sonnenschein R, Zebisch M, Marcantonio M, Ricotta C, Tonon G (2019) Estimating tree species diversity from space in an alpine conifer forest: The Rao's Q diversity index meets the spectral variation hypothesis. *Ecological Informatics*, **52**, 26–34.

Torresani M, Rossi C, Perrone M, *et al.* (2024) Reviewing the Spectral Variation Hypothesis: Twenty years in the tumultuous sea of biodiversity estimation by remote sensing. *Ecological Informatics*, **82**, 102702.

Viljur ML, Abella SR, Adámek M, *et al.* (2022) The effect of natural disturbances on forest biodiversity: An ecological synthesis. *Biological Reviews*, **97**, 1930–1947.

Villéger S, Mason NWH, Mouillot D (2008) New Multidimensional Functional Diversity Indices for a Multifaceted Framework in Functional Ecology. *Ecology*, **89**, 2290–2301.

Viña A, Liu W, Zhou S, Huang J, Liu J (2016) Land surface phenology as an indicator of biodiversity patterns. *Ecological Indicators*, **64**, 281–288.

Violle C, Navas ML, Vile D, Kazakou E, Fortunel C, Hummel I, Garnier E (2007) Let the concept of trait be functional! *Oikos*, **116**, 882–892.

Vitkovskaya I, Batyrbayeva M, Spivak L (2016) The Estimate of the Spatial-Temporal Features of Vegetation Cover of Kazakhstan Based on Time Series Satellite Indeces in 2000–2015. *ISPRS - International Archives of the Photogrammetry, Remote Sensing and Spatial Information Sciences*, **XLI-B8**, 1067–1071.

Wang L, Qu JJ (2007) NMDI: A normalized multi-band drought index for monitoring soil and vegetation moisture with satellite remote sensing. *Geophysical Research Letters*, **34**.

Wang Q, Tenhunen J, Dinh NQ, Reichstein M, Vesala T, Keronen P (2004) Similarities in ground- and satellite-based NDVI time series and their relationship to physiological activity of a Scots pine forest in Finland. *Remote Sensing of Environment*, **93**, 225–237.

Wang R, Gamon JA (2019) Remote sensing of terrestrial plant biodiversity. *Remote Sensing of Environment*, **231**, 111218.

Wang R, Gamon JA, Cavender-Bares J (2022) Seasonal patterns of spectral diversity at leaf and canopy scales in the Cedar Creek prairie biodiversity experiment. *Remote Sensing of Environment*, **280**, 113169.

Weber D, Schwieder M, Ritter L, *et al.* (2023) Grassland-use intensity maps for Switzerland based on satellite time series: Challenges and opportunities for ecological applications. *Remote Sensing in Ecology and Conservation*.

Wenden B, Mariadassou M, Chmielewski FM, Vitasse Y (2020) Shifts in the temperature-sensitive periods for spring phenology in European beech and pedunculate oak clones across latitudes and over recent decades. *Global Change Biology*, **26**, 1808–1819.

White MA, De Beurs KM, Didan K, *et al.* (2009) Intercomparison, interpretation, and assessment of spring phenology in North America estimated from remote sensing for 1982–2006. *Global Change Biology*, **15**, 2335–2359.

Wong CYS, D'Odorico P, Arain MA, Ensminger I (2020) Tracking the phenology of photosynthesis using carotenoid-sensitive and near-infrared reflectance vegetation indices in a temperate evergreen and mixed deciduous forest. *New Phytologist*, **226**, 1682–1695.

Wu W, Xin Q (2022) A Global Annual Vegetation Phenology Dataset Derived from GIMMS LAI 3G Time Series for 1982–2015. *IGARSS 2022 - 2022 IEEE International Geoscience and Remote Sensing Symposium*, pp. 6130–6133.

Yuan Z, Ali A, Wang S, *et al.* (2019) Temporal stability of aboveground biomass is governed by species asynchrony in temperate forests. *Ecological Indicators*, **107**, 105661.

Zheng Z, Schmid B, Zeng Y, Schuman MC, Zhao D, Schaepman ME, Morsdorf F (2023) Remotely sensed functional diversity and its association with productivity in a subtropical forest. *Remote Sensing of Environment*, **290**, 113530.

Zhou Q, Sun X, Tian L, Li J, Li W (2020) Grouping-Based Time-Series Model for Monitoring of Fall Peak Coloration Dates Using Satellite Remote Sensing Data. *Remote Sensing*, **12**, 274.

Zhu Z, Wang S, Woodcock CE (2015) Improvement and expansion of the Fmask algorithm: Cloud, cloud shadow, and snow detection for Landsats 4–7, 8, and Sentinel 2 images. *Remote Sensing of Environment*, **159**, 269–277.